Nuclear Engineering and Design 409 (2023) 112347

Contents lists available at ScienceDirect

Nuclear Engineering and Design

journal homepage: www.elsevier.com/locate/nucengdes

Thermo-fluid dynamic analysis of HLM pool. Circe experiments

D. Martelli *, R. Marinari, I. Di Piazza, P. Lorusso, M. Tarantino

ENEA, Department of Fusion and Nuclear Safety Technology, 40032 Camugnano, BO, Italy

A B S T R A C T

This work reports a summary of the experimental and numerical activities performed to investigate thermal hydraulic phenomena occurring in response to hypothetical accidental scenarios of Protected Loss of Heat Sink (PLOHS), and Protected Loss of Flow (PLOFA) and the heat transfer in the lead–bismuth (LBE) cooled fuel pin bundle simulator (FPS) of the CIRCE facility.

A series of four experiments (PLOHS-PLOFA) were carried out simulating the total loss of the secondary circuit and the coolant pump trip with the subsequent simulation of the reactor scram (reduction of the electric power supplied to the fuel pin simulator) and activation of DHR system to remove the decay heat power (~5% of the nominal value).

Tests differ from each other by the applied boundary conditions such as the electrical power supplied to the Fuel Pin Simulator, the duration of the test, the power removed by the HX etc., while test #4 also differs for the forced circulation maintained after the simulation of the accidental transient.

In parallel experimental test were carried out to investigate the heat transfer in a wrapped, grid spaced FPS. The FPS is composed of 37 electrical pins placed on a hexagonal lattice with a pitch to diameter ratio of 1.8. The bundle is hosted in the CIRCE large pool facility and represents the hot source of the Integral Circulation Experiment (ICE) test section.

Several thermocouples (0.5 mm O.D.) are installed in the FPS to measure both clad and subchannel LBE temperatures at different ranks and two different sections. Experimental data are used to evaluate the Nu number in the Pe range 500–3000 and obtained data are compared with Ushakov and Mikityuk correlations having a validity range containing the experimental p/d ratio and for the selected Pe range.

Experimental data relating to the obtained Nu number and the thermal hydraulic phenomena such as the modification of the thermal stratification in “pool type” configuration, coolant mass flow rate adaptation in the test section occurring during the simulation of the designed accidental conditions and the capability to cool the FPS under natural circulation conditions are described in this paper. Finally, the experimental database was used for validation of the geometrical and numerical model of the FPS adopted for 3D CFD calculations. In the performed simulations a sensitivity analysis was carried out for the turbulent Prandtl number in the range between 1 and 3 and a comparison between the first order turbulence model k-ω SST and the higher order Reynolds Stress Model was accomplished.

1. Introduction

CIRCE (CIRColazione Eutectico) (Turroni, 2001) is a large scale LBE pool-type facility hosted at ENEA C.R. Brasimone (Italy), aiming at supporting the development of Liquid Metal Fast Reactors (LMFR). The system is conceived to reproduce the thermo-hydraulic behaviour of a pool type reactor cooled by heavy liquid metal (HLM) under normal and abnormal conditions analysing the response in terms of safety to the simulated accidental scenarios (Tarantino et al., 2015). Moreover, the presence of a fuel pin simulator composed of 37 rods electrically heated with a relevant power installed (~1MW) has enabled a greater understanding of heat transfer in fuel bundle configuration.

Additionally, the experimental outcomes constitute an important database for the verification and validation of new models and new software tools developed to investigate thermal-hydraulics issues related to HLM technology.

In the first part of this paper, the authors report the description of the experimental activity carried out on the CIRCE facility focusing on the Integral Circulation Experimental configuration of the test section (ICE, (Tarantino et al., 2015; Tarantino et al., 2011; Martelli et al., 2019) operated in the frame of the European H2020 project Safety Assessment of Metal cooled reactor (SESAME, (sesame-h2020, xxxx; Martelli, xxxx).

In the second part of the paper, the experimental and numerical thermal investigation of the fuel pin simulator is reported.

2. Circe-ICE

CIRCE is a non-nuclear (electrical) experimental platform in a scale representative of the pool-type LFRs. The main vessel is a cylindrical vessel (1200 mm outer diameter, 8500 mm height and 15 mm thickness) designed to withstand a temperature of 500 °C and a pressure of 15 bar. The working primary fluid is lead–bismuth eutectic (LBE) and the

* Corresponding author.
E-mail address: daniele.martelli@enea.it (D. Martelli).

https://doi.org/10.1016/j.nucengdes.2023.112347
Received 16 December 2022; Received in revised form 18 April 2023; Accepted 19 April 2023
Available online 29 April 2023

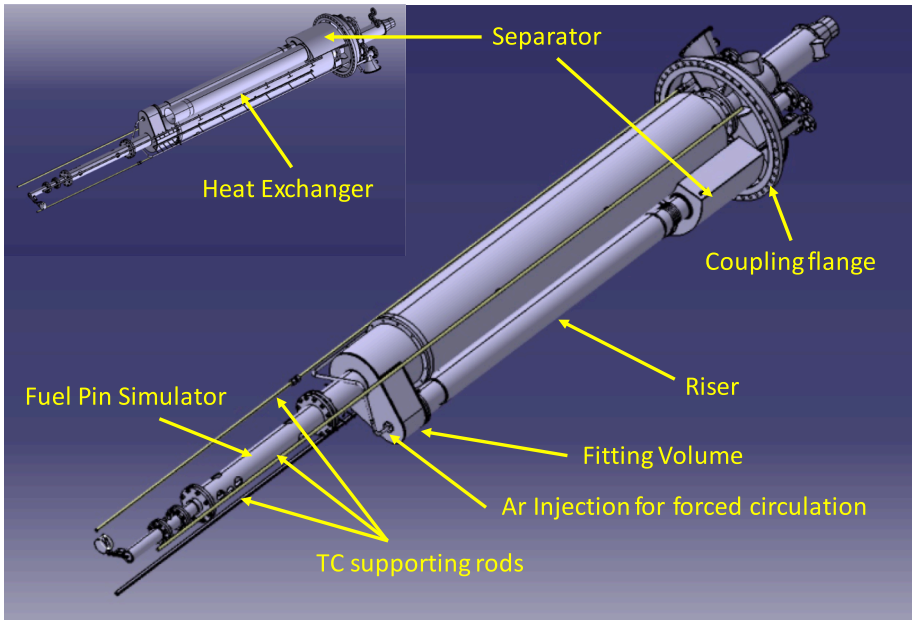

Fig. 1. CIRCE ICE Test Section.

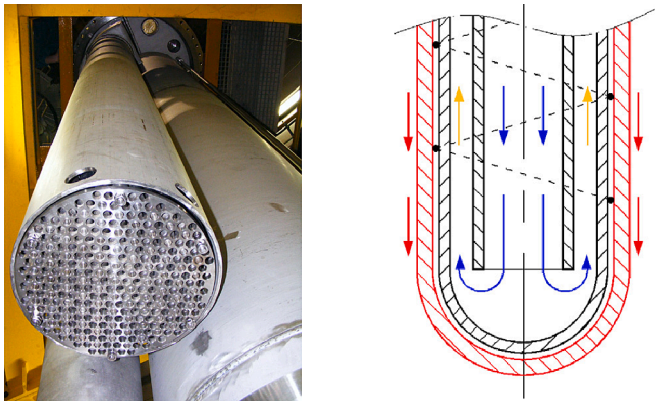

Fig. 2. View of the ICE HX installed into the test section (left) and Sketch of the bayonet tubes (right).

maximum inventory is 90 tons. The external walls of the main vessel are insulated by rock wool to minimize the thermal losses toward the environment and electrical heating cables are installed all around its bottom and lateral surfaces to avoid LBE freezing. The cover gas of the main vessel is also equipped with an automatic discharge system and passive pressure safety system (rupture disks), to prevent accidental overpressure in case of a steam generator tube rupture. Other two vessels are used for storage of the LBE during maintenance and refurbishment of the facility (S200) and for filling and drain procedures (S300).

The argon recirculation system, used to inject Ar gas for promoting the forced circulation, is equipped with a set of 5 compressors connected in parallel and an argon storage tank, acting as gas lung and directly connected to external gas tanks used for argon re-integration.

The S100 main vessel is conceived to host different test sections (TS) connected to the S100 using a flanged connection at the top of the vessel. In the experimental campaigns here described the ICE test section was installed (Fig. 1). It was designed to reproduce the thermal hydraulic behaviour of the primary system of a pool type Heavy Liquid Metal Cooled (HLMC) reactor. The heating source of the ICE TS is represented by a fuel pin simulator electrically heated composed of 37 pins. Each pin has an outer diameter of 8.2 mm and an active length of 1000 mm. The linear power is 25 kW/m with a maximum wall heat flux of 1 MW/m^2 and a total electrical power of 925 kW. Such large fuel pin lattice reduces the pressure losses and hence facilitates the establishment of coolant natural circulation for the long term coolability of the fuel assembly (larger values are used in HLM concept thanks to the coolant characteristics of low-moderating medium and low-adsorption cross section). The heated LBE flows upward in the riser up to the separator acting as a hot pool. This component is used also to separate the gas injected at the bottom of the riser for promoting the forced circulation (gas enhanced circulation) and connect the primary system to the heat exchanger (HX).

The heat exchanger in the ICE configuration is a bayonet tube HX (Fig. 2). The LBE flows in the shell side while water at low pressure flows in the tube side and the steam vent piping collects the steam from the tube bundle and discharges it into the atmosphere. The HX is made of 91 bayonet tubes (Fig. 2 right) consisting of three concentric tubes. The water flows downward in the inner pipes, and then upward in the annulus between the inner and intermediate pipes. Vaporization takes place in the ascending annulus avoiding the formation of flow instabilities. The annulus between the middle and outer pipes is filled by pressurized helium (4.5 bar) and used to detect any tube rupture monitoring the pressure in the common helium gas plenum. The HX is fed by water at ambient temperature and pressure.

The decay heat removal system (DHR) acts as heat sink of the system during the simulation of the HX failure (Loss of Heat Sink) for the long term coolability. It is hydraulically de-coupled by the primary system being placed into the downcomer. The DHR heat exchanger has been designed to have a thermal duty of 40 kW. It is a bayonet tube fed by air at atmospheric pressure (Fig. 3).

3. PLOHS-PLOFA experimental test matrix

The experimental activity consists of a series of four tests (named Test 1, Test 2, Test 3 and Test 4) simulating the total loss of the secondary circuit and the coolant pump trip (simulated by stopping the gas enhanced circulation, with the exception of Test 4) with the consequent reactor scram (reduction of the electric power supplied to the fuel pin simulator) and activation of DHR system to remove the decay heat power (~5% of the nominal value) (Martelli, xxxx). The boundary conditions of the performed tests are reported from Tables 1–4. Test 1, Test 2 and Test 3 differs in the thermal power supplied to the fuel pin simulator and consequently in the power removed by the heat exchanger

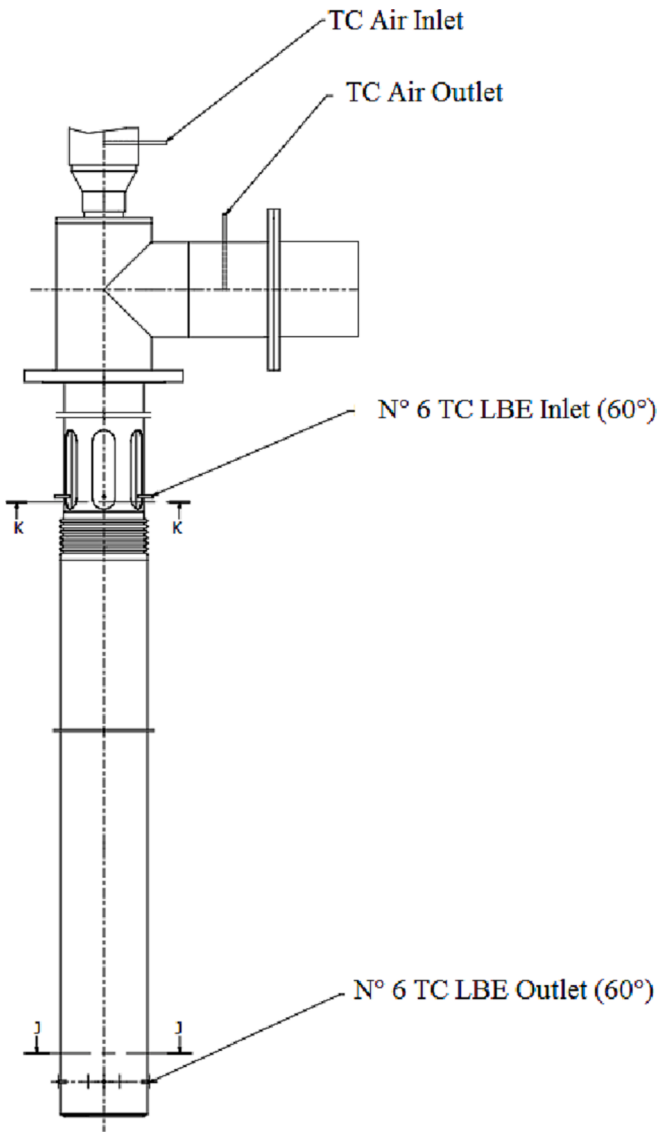

Fig. 3. Decay Heat Removal system.

Table 1
Boundary conditions for TEST 1.

Nominal Steady State	PLOHS + LOF transient
HS Thermal Power ~ 800 kW	Isolation of the main HX (isolating the feed water)
HLM flow rate: 60–70 kg/s (by gas lift)	Core "scram" at about 30 kW (decay power)
Argon mass flow rate ~ 3Nl/s	Start-up of the DHR-system (air mass flow rate 0.24 kg/s)
Average velocity into the HS:1m/s	DHR air inlet @ room temperature
Pool LBE initial temperature ~ 314 °C (Vertical gradient in the pool of 3 °C 316 T-MS-001, 312 °C T-MS-119)	"Main pump" turn-off (the gas injection is interrupted)
Vessel heating system: not active	Vessel heating system: not-active
HX water flow rate ~ 0.6 kg/s	
HX thermal power removed ~ 750 kW	
DHR: not active	
HX inlet Water @ room temperature	

Table 2
Boundary conditions for TEST 2.

Nominal Steady State	PLOHS + LOF transient
HS Thermal Power ~ 600 kW	Isolation of the main HX (isolating the feed water)
HLM flow rate: 60–70 kg/s (by gas lift)	Core "scram" at about 30 kW (decay power)
Argon mass flow rate ~ 2.4 Nl/s	Start-up of the DHR-system (air mass flow rate $\dot{m} \sim 0.325/0.22KG/S$)
Average velocity into the HS:1m/s	DHR air inlet @ room temperature
Pool LBE initial temperature ~ 280 °C (Vertical gradient in the pool of 4 °C 282 T-MS-001, 278 °C T-MS-119)	"Main pump" turn-off (the gas injection is interrupted)
Vessel heating system: not active	Vessel heating system: not-active
HX water flow rate ~ 0.5 kg/s	
HX thermal power removed ~ 510 kW	
DHR: not active	
HX inlet Water @ room temperature	

Table 3
Boundary conditions for TEST 3.

Nominal Steady State	PLOHS + LOF transient
HS Thermal Power ~ 750 kW	Isolation of the main HX (isolating the feed water)
HLM flow rate: 59.6 kg/s (by gas lift)	Core "scram" at about 30 kW (decay power)
Argon mass flow rate ~ 2.5–2.6 Nl/s	Start-up of the DHR-system (air mass flow rate 0.2 kg/s)
Average velocity into the HS: 0.91 m/s	DHR air inlet @ room temperature
Pool LBE initial temperature ~ 270 °C (Vertical gradient in the pool of 1–2 °C)	"Main pump" turn-off (the gas injection is interrupted)
Vessel heating system: not active	Vessel heating system: not-active
HX water flow rate ~ 0. 5 kg/s	
HX thermal power removed ~ 411 kW	
DHR: not active	
HX inlet Water @ room temperature	

Table 4
Boundary conditions for TEST 4.

Nominal Steady State	PLOHS transient
HS Thermal Power ~ 750 kW	Isolation of the main HX (isolating the feed water)
HLM flow rate: 59.6 kg/s (by gas lift)	Core "scram" at about 30 kW (decay power)
Argon mass flow rate ~ 2.5–2.6 Nl/s	Start-up of the DHR-system (air mass flow rate 0.2 kg/s)
Average velocity into the HS: 1 m/s	DHR air inlet @ room temperature
Pool LBE initial temperature ~ 280 °C (Vertical gradient in the pool of 4 °C)	Gas injection is NOT interrupted
Vessel heating system: not active	Vessel heating system: not-active
HX water flow rate ~ 0. 6 kg/s	
HX thermal power removed ~ 411 kW	
DHR: not active	
HX inlet Water @ room temperature	

and being the general outcomes similar, only those obtained in Test 2 are here described.

As shown in Table 4, Test 4 differs from the other tests in the fact that the forced circulation is maintained also after the transition to reduced power condition.

4. PLOHS-PLOFA experimental outcomes

For the sake of simplicity, only experimental data obtained for TEST 2 are presented while pointing out general outcomes and comments related to the entire experimental campaign.

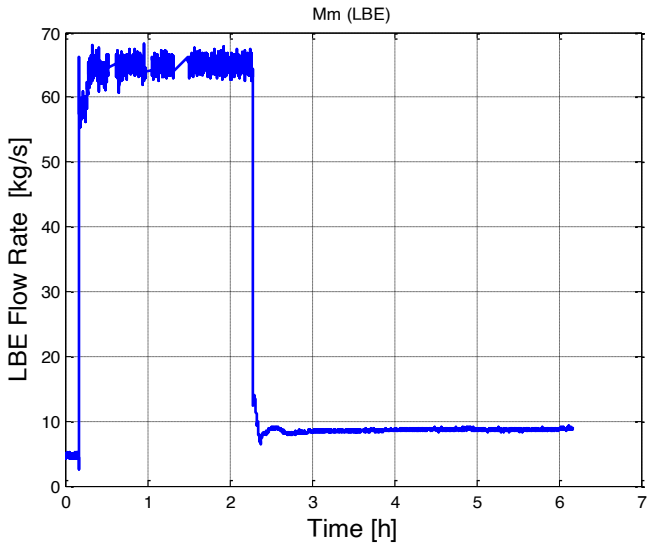

Fig. 4. TEST 2 LBE mass flow rate.

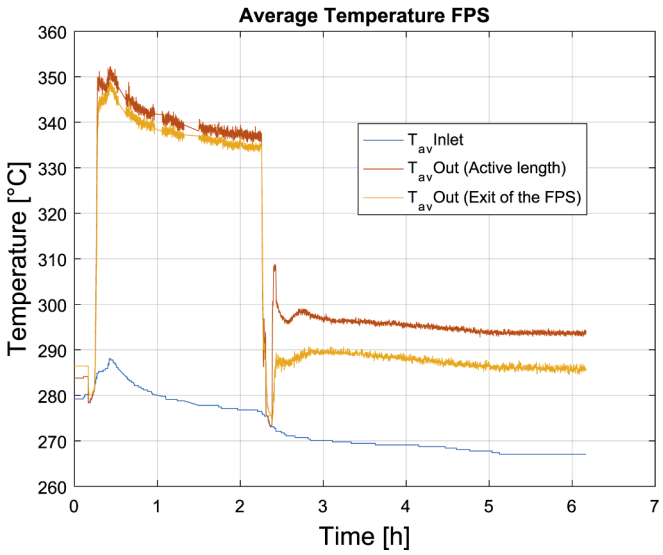

Fig. 6. Average temperatures in the FPS.

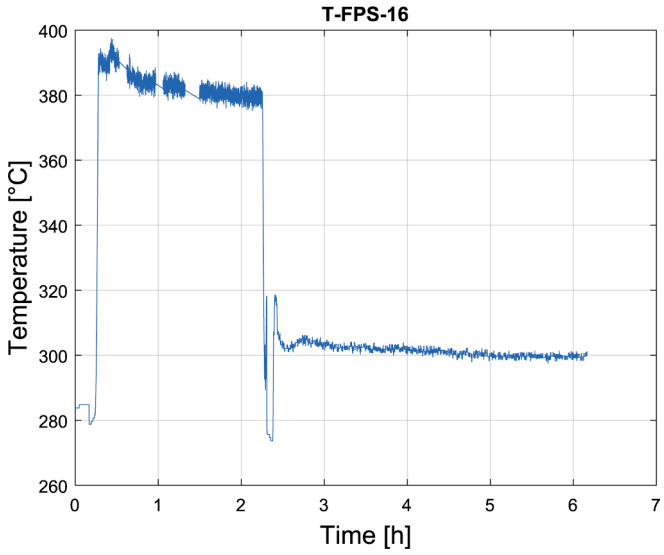

Fig. 5. TEST 2 Clad temperature on the central pin 60 mm upstream of the upper spacer grid.

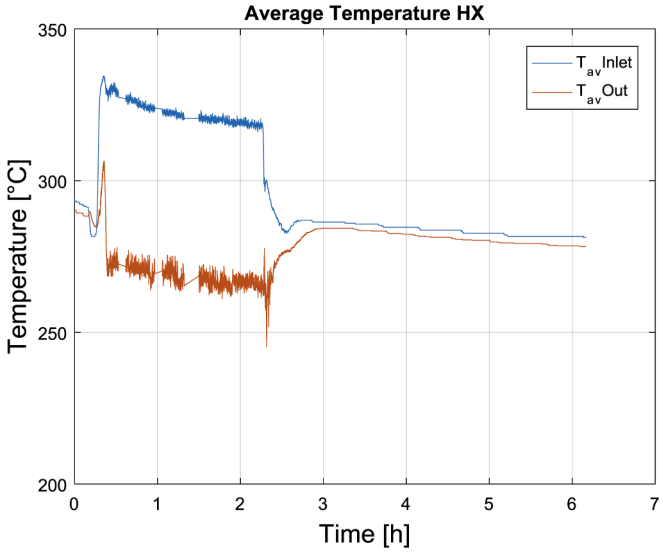

Fig. 7. Average temperatures in the HX (lead side).

Because of the simulated PLOHS-PLOFA accident, the LBE mass flow rate went from forced circulation to natural circulation conditions (Fig. 4).

At normal operating conditions with Ar injected into the riser to promote the LBE forced circulation the LBE mass flow rate is about 65 kg/s, oscillations in the measured value are the consequence of the oscillation of Ar bubble injected into the riser. After the simulation of the pump trip, simulated deactivating the Ar injection system, the LBE flow in the test section reaches a new steady state under natural circulation with a mass flow rate of about 9 kg/s. The pin clad temperature during the transition from forced to natural circulation should represent a major concern for the integrity of the pin. Nevertheless, the sudden reduction of the power supplied to the fuel pin simulator mitigates the problem and considering the temperature of the clad in the central pin (Fig. 5) the values decrease from 380 °C during the normal operation (800 kW) to about 300 °C at the new steady state at low power (30 kW) with an overshoot of about 20 °C (320 °C) while the natural circulation was establishing.

A similar trend is depicted in Fig. 6 for the LBE temperature at the exit of the active length. In normal operating conditions the LBE thermal gradient across the active length of the FPS is about 60 °C in TEST 2 and decreases to about 25 °C after the reduction of the power and transition to natural circulation. In normal operating condition, LBE enters the HX shell side at about 325 °C and exits at about 270 °C (Fig. 7), transferring about 510 kW to the water flowing in the HX. After the simulated transient the HX water flow rate is deactivated and the temperature gradient between the inlet and outlet section of the HX of about 5 °C is essentially due to heat losses toward the pool. In normal conditions, the average water flow rate on the secondary side in normal condition is 0.5 kg/s.

After the PLOHS-PLOFA transient, the decay heat removal system is activated injecting an air flow rate of about 325 g/s in the DHR (then reduced at 220 g/s after about 5 h, to reduce the power removed). The thermal power removed by the DHR was about 25 kW (air flow rate @325 g/s) and then reduced to 20 kW by reducing the air flow rate feeding the DHR (Fig. 8).

Several thermocouples are installed in the pool for the investigation of mixing and stratification phenomena. Thermocouples are fixed to vertical supporting rods (nine supporting rods radially distributed into

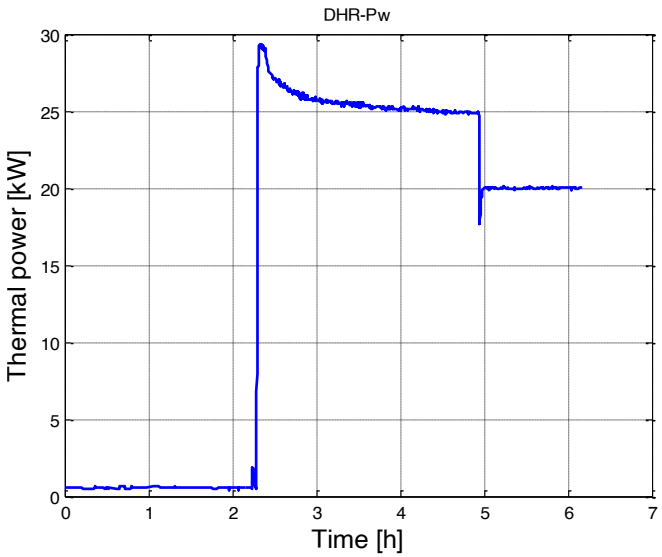

Fig. 8. Power removed by the DHR system.

the pool) at seventeen different elevations (for a detailed description of the instrumentations see (Tarantino et al., 2015). Lines A and H permit to measure the temperature in the pool along the entire length of the test section.

During the normal operation phase, the thermal gradient covers the whole pool ranging from about 322 °C at the top part of the pool to 277 °C in the lower parts (inlet section of the TS; Fig. 9).

After the start of the simulation of the PLOHS-PLOFA accident (about 2.2 h), a relevant modification of the thermal gradient in the pool occurs which results in the formation of two regions of uniform temperature (upper and lower plenum, essentially) separated by a thin region (less than 1 m) where the thermal gradient is steepest. No radial temperature variation was observed.

The main difference obtained in TEST 4 compared to the other tests is in the thermal stratification. Indeed, due to the different accidental scenarios simulated (PLOHS without a loss of flow) the temperature in the pool becomes uniform because the forced circulation is still running after the loss of the HX.

5. Heat transfer in the circe fuel bundle

A dedicated experimental campaign was performed for the characterization of forced and mixed convection in HLM coolant. Indeed, liquid metals have a relatively low Pr with respect to water (Pr ≪ 1) consequently, the thermal transport is much larger than that of momentum and therefore the thermal and viscous boundary layers are not of the same order of magnitude.

Most of the different experimental work available in HLM scientific literature deals with sodium–potassium alloy (NaK of different

Table 5
Boundary conditions for FC & NC experimental tests.

Name	LBE Mass flow rate [kg/s]	Argon Mass flow rate [Nl/s]	FPS Electrical Power [kW]	ΔT (outlet-inlet) FPS [°C]
1-FC	70	5.00	800	80
2-FC	65	4.40	760	80
3-FC	60	3.00	700	80
4-FC	55	2.40	640	80
5-FC	50	1.60	580	80
6-FC	45	1.45	525	80
7-FC	40	1.41	465	80
1-NC	25	0	600	165
2-NC	23	0	500	151
3-NC	21	0	400	133
4-NC	19	0	300	109
5-NC	14	0	200	102
6-NC	12	0	100	58

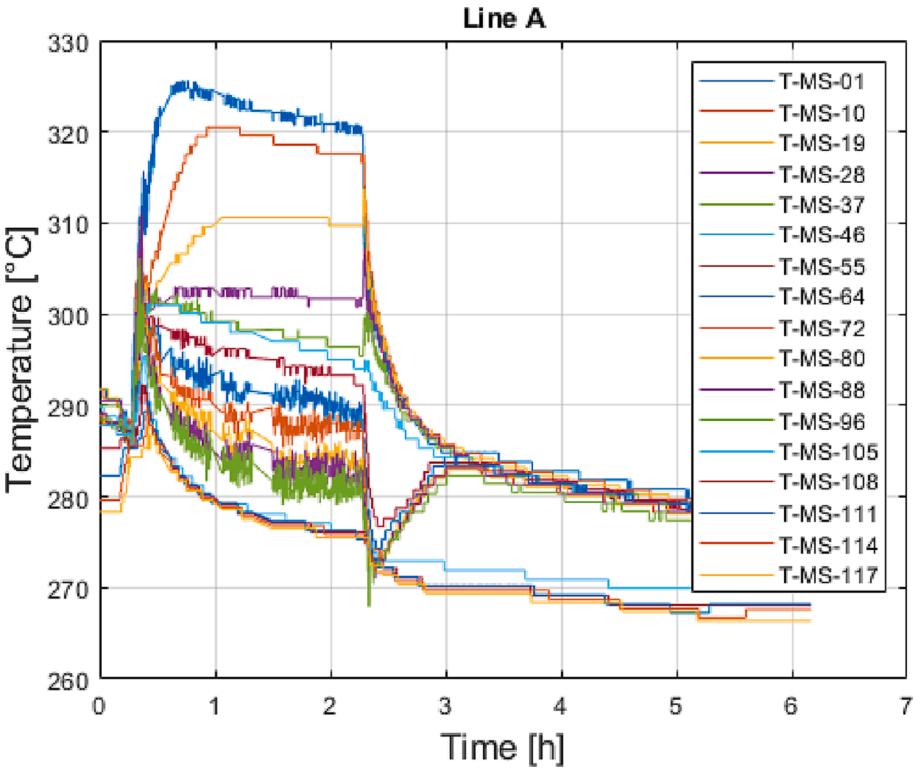

Fig. 9. LBE Thermal gradient in the pool.

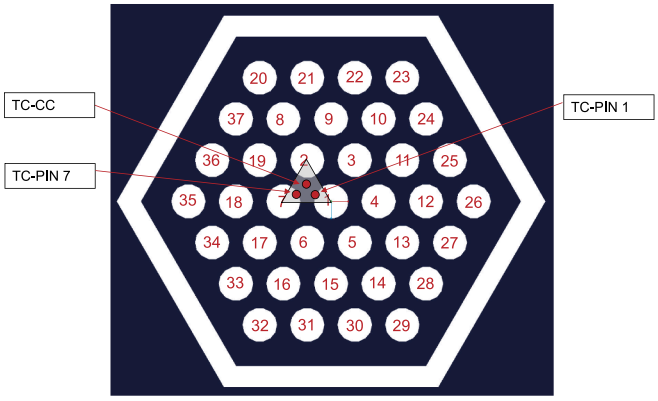

Fig. 10. Measurement points of temperature in the central subchannel.

composition) or mercury (Hg) as reference fluid (Mikityuk, 2009). Therefore, specific experimental tests with Lead and Lead Bismuth Eutectic alloy (LBE) are mandatory in support of the LFR core thermal-hydraulics design.

For a complete description of the geometry and instrumentation of the fuel pin bundle of the CIRCE ICE test section refer to (Martelli et al., 2015). All the experimental data reported in Table 5 refers to the central subchannel of the FPS surrounded by pins 1,2 and 7 of section 1 and section 3 (Fig. 10) placed at 20 mm upstream of the middle spacer grid and 60 mm upstream of the upper spacer grid, respectively.

Two series of tests were carried out: forced and natural circulation. Tests in forced circulation conditions were performed imposing a thermal difference through the FPS of about 80 °C and the electrical power to be supplied to the FPS was calculated by a balance equation imposing the desired LBE mass flow rate through the FPS. During this test, subchannel temperatures were investigated at different Peclet numbers by changing the LBE mass flow rate from a value of about 40 kg/s to 70 kg/s with a step of about 5 kg/s. For each step steady state temperature conditions in the FPS were reached and maintained at least for 15 min and the Nusselt number was evaluated. Tests in natural circulation condition were performed to obtain Nusselt number at lower Peclet numbers. During these tests the electrical power supplied to the FPS was varied from 100 kW to 600 kW with steps of 100 kW, obtaining an LBE mass flow rate range from 12 kg/s to 25 kg/s (Table 5).

The primary variables measured during the experimental tests are temperatures and LBE mass flow rate. Temperatures were monitored at two different sections along the active length named Section 1 and 3.

Temperatures are measured in the central subchannel as a reasonable approximation to an infinite lattice for comparison with available correlations for HLM. Moreover, the bulk temperature used in the evaluation of the Nu is obtained assuming a linear temperature profile between the entrance and exit of the FPS active length. The measured temperatures of the pin clad are corrected for the thermal conduction in the probe thickness to consider the position of the thermocouple fixed to the pin external wall with an AISI 304 sheet.

Fig. 11 shows the Nu results obtained for Test 1 FC and Test 1 NC at

Table 6
Nu & Pe evaluated from the experimental data with their uncertainties.

	Section 1				Section 3			
Name	Pe	$\langle\frac{\sigma_X}{X}\rangle$	Nu	$\langle\frac{\sigma_X}{X}\rangle$	Pe	$\langle\frac{\sigma_X}{X}\rangle$	Nu	$\langle\frac{\sigma_X}{X}\rangle$
1-FC	2933	9%	26.3	10.0%	2812	9%	24.5	9.3%
2-FC	2772	9%	25.8	10.1%	2657	9%	23.6	9.4%
3-FC	2572	9%	26.0	10.4%	2462	9%	23.0	9.8%
4-FC	2365	9%	23.9	10.5%	2266	9%	21.2	9.9%
5-FC	2122	10%	23.8	12.3%	2031	10%	21.1	11.4%
6-FC	1896	11%	23.0	15.3%	1811	11%	20.7	14.4%
7-FC	1776	12%	23.2	16.6%	1698	12%	20.6	16.0%
1-NC	984	9%	20.3	10.1%	903	9%	18.0	9.8%
2-NC	903	9%	20.0	10.3%	835	9%	17.4	9.9%
3-NC	796	9%	17.8	10.2%	745	9%	15.5	9.3%
4-NC	738	9%	17.7	9.9%	698	9%	14.3	9.7%
5-NC	579	9%	18.8	16.9%	548	9%	13.7	13.9%
6-NC	542	9%	17.2	13.2%	524	9%	12.5	12.9%

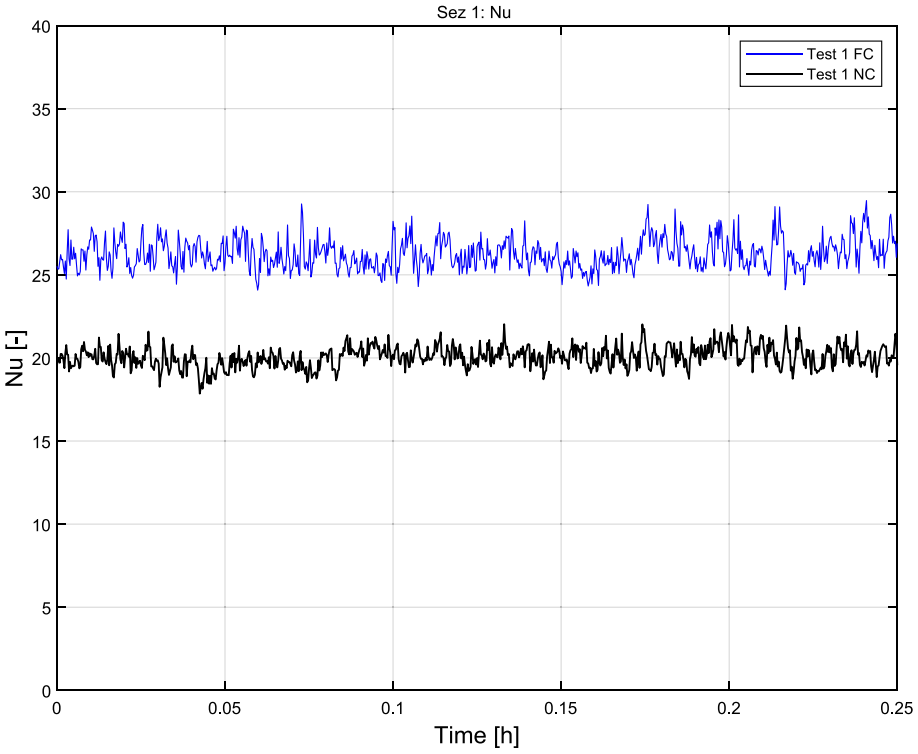

Fig. 11. Nu number central subchannel Test 1 FC and Test 1 NC.

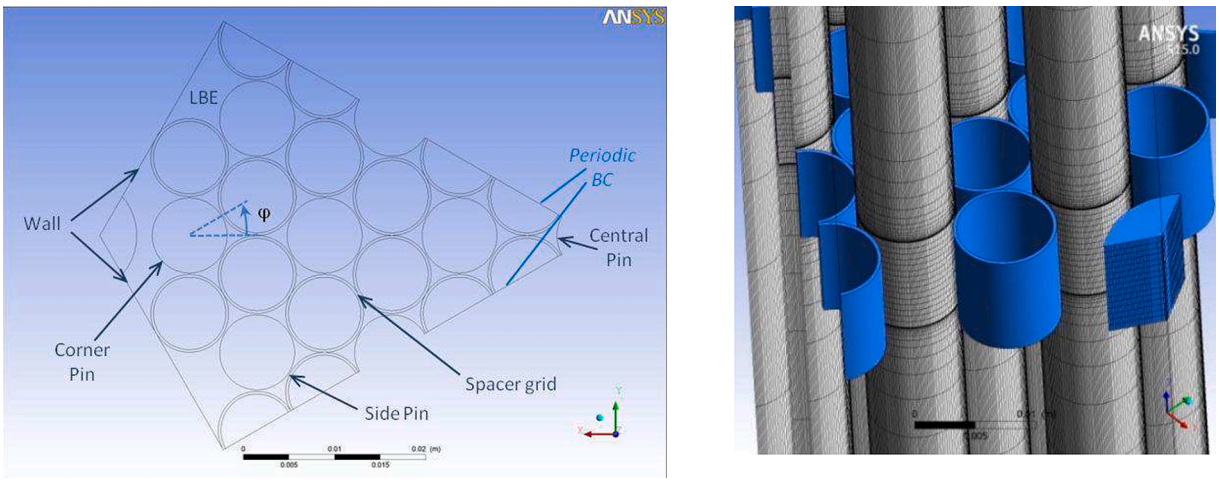

Fig. 12. Geometrical domain (left) and detail of the adopted discretization (right).

Table 7
Cases analysed for the mesh independence.

Name	y^+	N_{node}
$A_1 = B_3 = NOM$	1	$1.14{\cdot}10^7$
A_2	2	$1.14{\cdot}10^7$
A_3	8	$1.14{\cdot}10^7$
A_4	15	$1.14{\cdot}10^7$
B_1	1	$6.6{\cdot}10^6$
B_2	1	$8.0{\cdot}10^6$
$B_3 = A_1 = NOM$	1	$1.14{\cdot}10^7$
B_4	1	$1.50{\cdot}10^7$

the central subchannel of Section 1.

In Table 6 the Pe and Nu numbers obtained from the primary experimental data (i.e. LBE mass flow rate, LBE bulk temperature and pin temperature in the central subchannel) are reported together with their uncertainties obtained as the root-sum-of-squares of all partial error according to the Gaussian error propagation theory (Moffat, 1988).

This experimental data was used for the verification of CFD models adopted to simulate the CIRCE fuel pin simulator. Considering the symmetry of the geometry of the FPS, the model reproduced an angle of 60 °C with lateral rotational periodic boundary conditions (Fig. 12 left). Concerning the spatial discretization, a grid mesh independence assessment was carried out evaluating both Darcy–Weisbach friction factor and Nusselt number. Two series of mesh (A, B) have been tested; "A" type meshes differ in the number of cells near walls ($1 < y+ < 15$) while maintaining the total number of nodes in the whole domain. "B" type meshes have the same $y+ \sim 1$ at the walls and different number of computational nodes (Table 7).

Finally, to obtain the best compromise between resolution and computational time the discretization mesh $A_1 = B_3$ was selected. It is composed of about 11 million mesh elements, of which about 250,000 used for the discretization of the spacer grids (Fig. 12 right). The conjugate heat transfer in the spacer grid was also modelled.

A comparison between the first order turbulence models (SST k- ω) and the higher-order Reynolds Stress model (RSM) was carried out for the nominal case with $w_0 = 1$ m/s and q''=1 MW/m^2. The SST model did not predict significant secondary flows while the RSM model predicted a complex secondary circulation limited to the corner and side subchannels. Considering that CFD-Experimental comparison was focused on the inner subchannel (negligible influences of the secondary flow paths), the SST k- ω turbulence model was chosen for all the performed simulations to reduce the computational time and considering the fact that in terms of Nusselt number the difference with RSM model is negligible. Moreover, due to HLM's very large molecular thermal diffusivities, the Reynolds analogy ($Pr_t \sim 1$) is no longer valid and the default $Pr_t = 0.9$ used in the CFX solver would lead to incorrect heat transfer predictions. Therefore, a sensitivity study on the Pr_t was

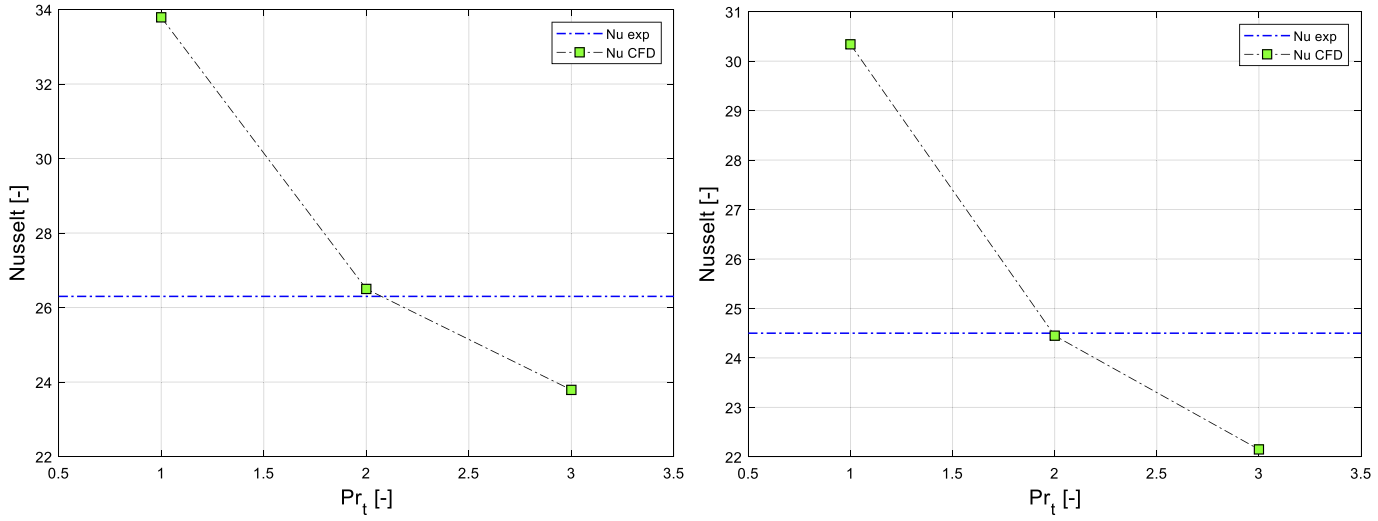

Fig. 13. Nu VS Pr_t Section 1 (left) and 3 (right).

Table 8
CFD Vs Experimental temperature comparison.

Name	$T_{bulk,\ CFD}$ [°C]	$T_{bulk,\ Exp}$ [°C]	$T_{pin,\ CFD}$ [°C]	$T_{pin,\ Exp}$ [°C]	$T_{CC,\ CFD}$ [°C]	$T_{CC,\ Exp}$ [°C]
Section 1						
1-FC	322.2	322.9	377.5	377.2	310.7	312.5
2-FC	320.1	320.7	374.1	373.0	309.0	311.1
3-FC	309.5	310.1	361.0	359.1	298.6	300.4
4-FC	311.3	311.8	360.0	360.2	301.4	304.2
5-FC	305.6	306.1	351.8	350.3	296.4	297.9
6-FC	298.9	299.6	342.0	342.3	289.3	291.5
7-FC	292.3	292.9	331.5	331.2	283.4	285.1
1-NC	386.6	388.1	443.6	441.4	374.4	372.4
2-NC	388.0	389.4	436.8	434.3	378.0	376.0
3-NC	416.7	417.3	455.6	456.2	409.2	409.3
4-NC	403.7	404.0	434.4	434.1	398.1	398.6
5-NC	345.0	345.8	368.8	366.8	341.1	341.0
6-NC	310.4	310.8	323.3	322.8	308.3	309.1
Section 3						
1-FC	361.7	358.2	419.4	414.2	353.7	355.1
2-FC	359.8	356.1	415.1	411.4	352.3	352.7
3-FC	349.7	346.1	403.0	399.2	342.2	342.9
4-FC	351.0	347.3	401.9	399.7	344.6	348.0
5-FC	345.8	342.1	393.6	390.1	340.0	339.8
6-FC	340.4	337.2	384.8	383.3	334.1	334.8
7-FC	332.2	329.1	372.4	372.1	326.1	325.8
1-NC	476.8	468.1	536.0	523.9	471.4	464.8
2-NC	469.4	461.8	520.3	510.1	465.4	460.5
3-NC	487.7	480.6	529.1	522.8	485.2	482.7
4-NC	462.8	456.4	495.6	491.6	461.1	459.4
5-NC	399.6	394.5	425.7	421.8	399.2	397.8
6-NC	340.7	338.2	355.0	354.4	340.6	341.8

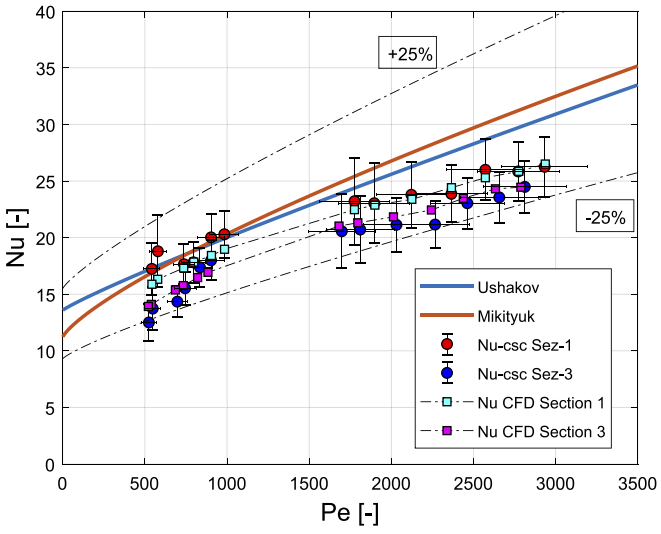

Fig. 14. Experimental and CFD Nu vs. Pe number and comparison with Mikityuk and Ushakov correlations.

performed assuming values in the range between 1 and 3 and the obtained Nu was compared with the one obtained from the experimental data Test 1FC (Fig. 13). Moreover, a variable Prandtl approach was also adopted implementing the Kays (Kays, 1994) correlation inside the CFX software. The comparison showed a good agreement for a constant $Pr_t = 2$ while for a variable Pr the experimental Nu was overestimated with a discrepancy of 15% for section 1 and 12% for section 3. Therefore, a constant $Pr_t = 2$ was adopted in all simulations.

CFD and experimental temperature values used for calculation of the Nu for all simulations are reported in Table 8 where the experimental wall temperature is obtained averaging temperatures measured on the walls of pin 1 and pin 7 (Fig. 10); moreover, this value is corrected in order to consider the position of the thermocouple fixed to the pin external wall with an AISI 304 sheet, the bulk temperature in the experiment is obtained considering a linear trend between the average temperature values at the entrance and at the exit of FPS active length and T_{cc} is the experimental temperature monitored in the centre of the subchannel.

The comparison presented in Fig. 14 between experimental data, CFD results and Nusselt number resulting from literature correlations (for circular rods arranged in a triangular lattice) (Mikityuk, 2009; Ushakov et al., 1977) showed a good agreement with a percentage error lower than 13% between experimental and CFD results and lower than 25% if compared with data from semi-empirical correlations.

Finally, Nu obtained from experimental data and from the simulations show a general trend that lies below the Nu obtained from Ushakov and Mikityuk. Empirical correlations are a useful tool for the thermal–hydraulic design of a fuel bundle and a good agreement with experimental data must be expected. Nevertheless, the experimental test must be considered as the reference for the specific geometry of the experimental fuel bundle analysed.

6. Conclusions

The main task of the experimental campaigns performed at ENEA using the Integral Circulation Experiment (ICE) was the investigation of the thermal–hydraulic behaviour of primary system of a pool-type nuclear reactor cooled by HLM. In particular, the experiments analysed were designed i) to investigate the transition from forced to natural circulation in a HLM pool-type system typically occurring in accident scenarios (PLOHS-PLOFA) with decay heat removed by the DHR-system, ii) to characterize the heat transfer in the HLM cooled fuel pin bundle and iii) to investigate in-pool thermal stratification phenomena.

The experiments allowed preliminary demonstration of long term coolability of the fuel bundle under natural circulation conditions. Furthermore, the simulated transient revealed the absence of high temperature peaks on the clad of the pins during the transient before the establishment of the LBE natural circulation.

Concerning the thermal stratification inside the pool at the full power steady state, the experiment showed the same general behaviour independent of the external conditions, characterized by the presence of a thermal gradient of about 40 °C in the first 3.5 m starting from the free LBE level to the outlet section of the HX. Then, between the outlet sections of the HX and the DHR, the slope of the vertical temperature profile increases, with a temperature drop of about 15–20 °C in less than 1 m. Moreover, the thermal stratification in the pool is purely vertical with negligible radial temperature variation. After the transition to natural circulation, the vertical temperature profile changes. In the upper and lower part of the vessel the LBE temperature is uniform within each zone, with a thin layer separating the two zones where the thermal gradient is steepest. That layer moved downwards below the DHR outlet section after the transition from forced to natural circulation and the temperature drop in the layer is reduced to about 10 °C.

Concerning the experimental activity carried out for the analysis of heat transfer in a 37-pin fuel rod bundle, Nu values obtained from the experimental data shows a linear trend as a function of the Pe, in agreement with Mikityuk and Ushakov correlations. In particular, the experimental Nu values differ from Nu obtained from Mikityuk and Ushakov correlations by less than 25%. This experimental data was used for tuning and verify the physical model created for CFD numerical simulation of the ICE FPS.

The CFD model, considering the physical symmetry of the geometry, represents a 60° slice with lateral rotational periodic boundary conditions. To evaluate the grid independence both Darcy–Weisbach friction factor and Nusselt number were considered. The adopted mesh is comprised of 11 million structured elements with near wall refinements (y+=1). The effects on the temperature field of the secondary circulation flows were investigated by invoking the RSM and the (SST) k- ω model. Temperature discrepancies were found to be relevant in the

corner sub-channels but negligible in the inner sub-channels where experimental attention was focused. Accordingly, to reduce the computational time, the Shear Stress Transport (SST) k- ω model was selected for all runs. A sensitivity study on the Pr_t was performed by assuming a constant and variable (Kays correlation) Pr_t numbers.

The predicted Nu number in the simulation with the variable Pr_t number with the k- ω turbulence model overestimated the Nu number obtained from the experimental data. Furthermore, the sensitivity study with a constant Pr_t number showed that the Nu number obtained from the numerical simulation with $Pr_t = 2$ was in good agreement with the one calculated from the experimental data.

The comparison of CFD results with Nu calculated from the experimental data shows a good agreement with an error less than 13%. Nu calculated from experimental and numerical simulation is likely to overestimate the Nu obtained from the Ushakov and Mikityuk correlations within ± 25%.

CRediT authorship contribution statement

D. Martelli: Writing – review & editing, Conceptualization. **R. Marinari:** Writing – review & editing. **I. Di Piazza:** Supervision, Conceptualization. **P. Lorusso:** Writing – review & editing. **M. Tarantino:** Project administration, Resources.

Declaration of Competing Interest

The authors declare that they have no known competing financial interests or personal relationships that could have appeared to influence the work reported in this paper.

Data availability

Data will be made available on request.

Acknowledgements

The work described in this paper summarizes the European collaborative efforts from the following projects which have received funding from the Euratom research and training program under grant agreements, No. 516520 (EUROTRANS), No. 249337 (THINS), No. 662186 (MYRTE), No. 654935 (SESAME). The work described in this paper was funded also by the Italian Minister for Economic Development (MiSE) in the framework of the FRAMEWORK AGREEMENT (ADP) MiSE-ENEA (2010-2018). The views and opinions expressed herein do not necessarily reflect those of the European Commission or the Italian Government.

The authors wish to acknowledge the input and contributions of all international colleagues involved. The authors wish to thank all the ENEA's technicians involved in the implementation and operation of the LFR R&D program.

References

Kays, W.M., 1994. Turbulent Prandtl number – where are we. J Heat Transf. Trans ASME 116 (2), 284–295.

Martelli, D., Forgione, N., Di Piazza, I., Tarantino, M., 2015. HLM fuel pin bundle experiments in the CIRCE pool facility. Nucl. Eng. Des. 292, 76–86.

Martelli, D., Forgione, N., Tarantino, M., 2019. CIRCE-ICE PLOHS experimental campaign. Nucl. Eng. Des. 355, 110307.

D. Martelli, V. Moreau, K. Zwijsen, "CIRCE experiments: pre-Test, data-set and analysis" deliverable D3.2 SESAME.

Mikityuk, K., 2009. Heat transfer to liquid metal: review of data and correlations for tube bundles. Nucl. Eng. Des. 239, 680–687.

Moffat, R.J., 1988. Describing the uncertainties in experimental results. Exp. Therm. Fluid Sci. 1 (1), 3–17.

https://sesame-h2020.eu/.

Tarantino, M., Agostini, P., Benamati, G., Coccoluto, G., Gaggini, P., Labanti, V., Venturi, G., Class, A., Liftin, K., Forgione, N., Moreau, V., 2011. Integral Circulation experiment: Thermal-hydraulic simulator of heavy liquid metal reactor. J. Nucl. Mater. 415, 433–448.

Tarantino, M., Martelli, D., Barone, G., Di Piazza, I., Forgione, N., 2015. Mixed Convection and stratification phenomena in a heavy liquid metal pool. Nucl. Eng. Des. 286, 261–277.

P. Turroni, L. Cinotti , G. Corsini, L. Mansani, "The CIRCE Facility", AccApp'01&ADTTA'01, Nuclear Application in the new Millennium, Reno (Nevada-USA), November 11-15, 2001.

P.A. Ushakov, A.V. Zhukov, M.M. Matyukhin, "Heat transfer to liquid metals in regular arrays of fuel elements, High Temperature", Vol. 15, pp. 868–873, 1977; translated from Teplofizika Vysokikh Temperatur 15 (5), pp. 1027–1033, 1977.